Fig. 2 ~ Fig. 4 show the comparison of the membrane water contents (λ), net water flux per proton (α) and current density distributions at averaged current density of 0.6 A/cm^2.

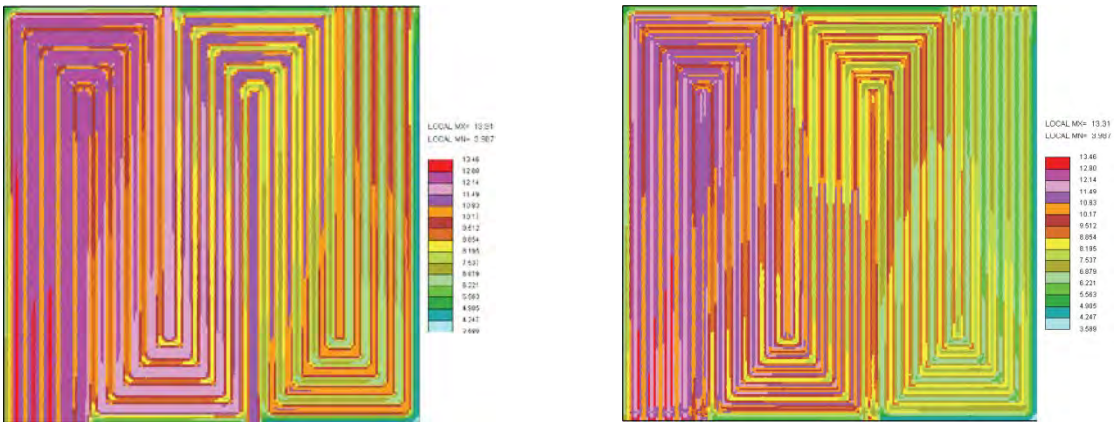

(a) case #1 (b) case #2

Fig. 2. Water content (λ) at I_{ave}=0.6 A/cm^2; (a) case #1; (b) case #2.

Fig. 2 shows the comparison of the membrane water contents between the case #1 and case #2 at the averaged current density of 0.6 A/cm^2. The membrane water content under the rib area is higher than that under the adjacent channel area because a lot of water produced at the cathode under the rib region can be absorbed into the membrane as shown in case #1. On the other hand, the membrane water content of the case #2 has smaller variation between the channel and rib than that of the case #1 because under-rib convection flow from channel to the adjacent rib and then flow from the inlet channel to the adjacent outlet channel, and liquid water gathers and discharges into sub-channel.

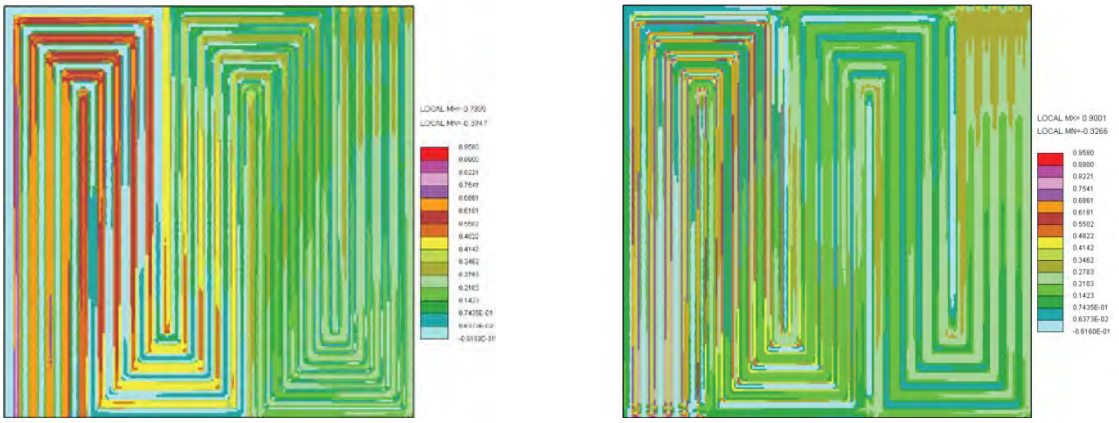

(a) case #1 (b) case #2

Fig. 3. Net water flux per proton (α) at I_{ave}=0.6 A/cm^2; (a) case #1; (b) case #2.

Fig. 3 shows the comparison of the net water flux per proton between the case #1 and case #2 at the averaged current density of 0.6 A/cm^2. The net water flux per proton is greater than 0 at the ribs and that is less than 0 at the channels as shown in case #1. The net water flux per proton is always greater than at the ribs because the hydrogen ions are transported from cathode to the anode with a lot of water. Case #2 shows that the net water flux per proton at the ribs is lower due to sub-channel than the net water flux per proton at the channels i.e. a lot of water is transported from cathode to the anode.

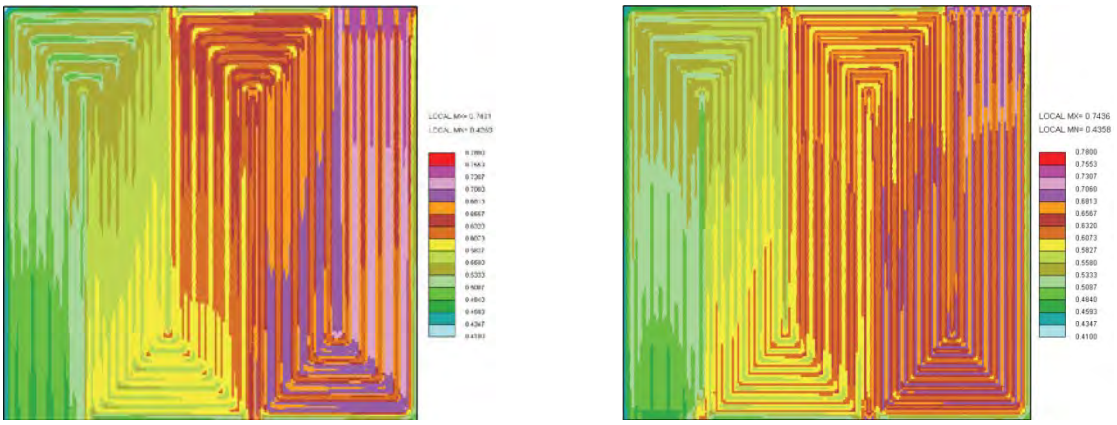

(a) case #1 (b) case #2

Fig. 4. Current density distributions at I_{ave}=0.6 A/cm^2; (a) case #1, case #2.

Fig. 4 presents the comparison of the current density distributions between the case #1 and case #2 at the averaged current density of 0.6 A/cm^2. The overall distributions show that the local current density is decreasing from the inlet toward the outlet due to the consumption of the reacting gases. Through the supplement of sub channel flow field, it is shown from the results that water removal characteristic inside channel improves because the flow direction of under-rib convection is changed into the sub channel. Therefore, case #2 shows that total current density distributions become uniform because retention time of reacting gases traveling to sub channel flow field is longer than to main channel.

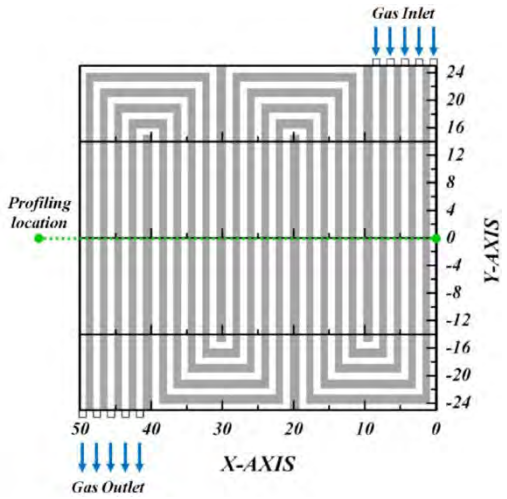

Fig. 5. Index and location of the serpentine flow-field.

Fig. 6 shows the comparison of the total pressures between the case #1 and case #2 at the averaged current density of 0.6 A/cm^2 and the same location as shown in Fig. 5. The pressure drops on the anode and cathode side for case #2 are 0.282 kPa and 1.321 kPa which are decreased by about 22.95 % and 17.12 % compared with 0.366 kPa and 1.594 kPa for case #1, respectively. The enhanced under-rib convection in both anode and cathode of case #2 decreases the pressure drop, which also contributes to the performance by reducing the power consumption of air blower.

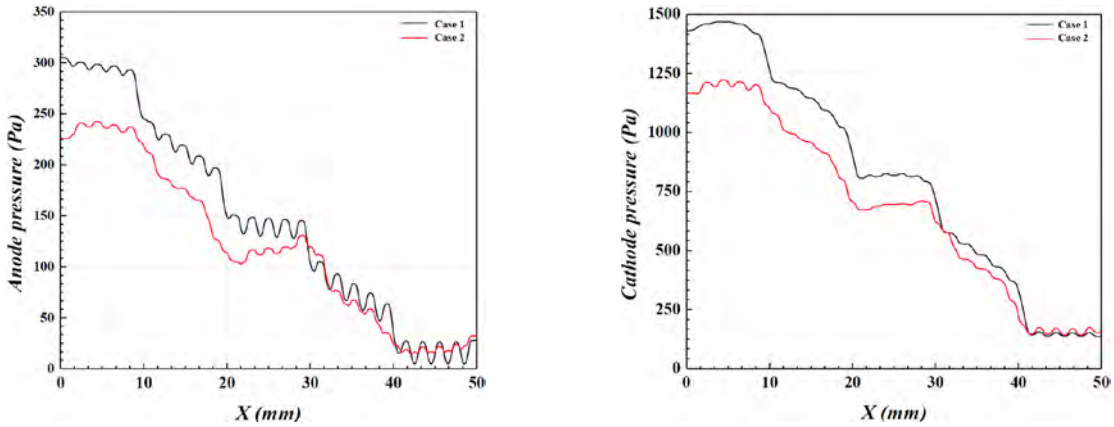

(a) Anode side (b) Cathode side

Fig. 6. The comparison of the total pressures between the case #1 and case #2 at I_{ave}=0.6 A/cm^2; (a) Anode side; (b) Cathode side.

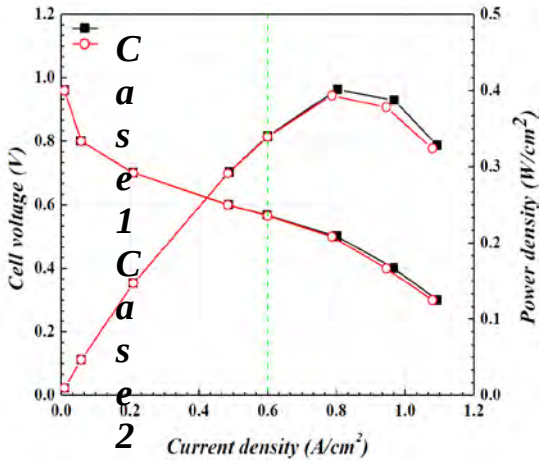

Fig. 7. The comparison of the polarization and power density curves between the case #1 and case #2.

To verify the maximization of power density among the performance-related parameters, the comparison of the polarization and power density curves between the case #1 and case #2 is given in Fig. 7. For the current density lower than 0.6 A/cm^2, the cell voltage and power density is independent of serpentine flow-field with and without sub-channel. For the current density greater than 0.6 A/cm^2, the cell voltages and power densities of case #1 and case #2 differ, the differences increase with the decreasing current density.

4. Conclusions

This study presents numerical analysis-based design of the serpentine flow field patterns to stimulate under-rib convection by adding sub-channel for improving the PEMFC performance. In the case of the case #2, under-rib convection flow from channel to the adjacent rib and then flow from the inlet channel to the adjacent outlet channel, and liquid water gathers and discharges into the sub-channel. Through the present numerical analysis-based design, the serpentine flow field with sub-channel enhances the performances of pressure drop, discharge of liquid water, and uniformities of current density.

Acknowledgements

This research was supported by Basic Science Research Program through the National Research Foundation of Korea (NRF) funded by the Ministry of Education, Science and Technology (No. 2009-0080496).

References

[1] F. Barbir, PEM Fuel Cells: Theory and Practice, Elsevier Academic Press, 2005.

[2] T. Kanezaki, X. Li and J.J. Baschuk, Cross-leakage flow between adjacent flow channels in PEM fuel cells, J. Power Sources 162, 2006, pp. 415 – 425.

[3] J.H. Nam, K.J. Lee, S.Sohn, C.H. Kim, Multi-pass serpentine flow-fields to enhance under-rib convection in polymer electrolyte membrane fuel cells: Design and geometrical characterization, J. Power Sources 188, 2009, pp. 14 – 23.

[4] D.H. Jeon, S. Greenway, S. shimpalee and J.W. Van Zee, The Effect of Serpentine Flow Field Designs on PEM Fuel Cell Performance, Int. J. Hydrogen Energy 33, 2008, pp. 1052 – 1066

[5] CD-adapco, ES-PEMFC Methodology and Tutorial Manual, CD-adapco Group, 2008, http://www.adapco.com.